DOI: 10.1002/adma.200701973

Strategies for Optimized Radiolabeling of Nanoparticles for *in vivo* PET Imaging**

By *Guorong Sun*, *Jinqi Xu*, *Aviv Hagooly*, *Raffaella Rossin*, *Zicheng Li*, *Dennis A. Moore*, *Craig J. Hawker*, *Michael J. Welch*,* and *Karen L. Wooley**

Driven by the motivation for optimizing ^{64}Cu radiolabeling efficiency of nanoparticles for *in vivo* positron emission tomography (PET) imaging, a new strategy has been developed. This strategy involved a complete redesign of the nanoparticle system, utilizing macromolecular precursors that were preloaded with labeling sites and programmed for supramolecular assembly into discrete, functional nanoscale objects. A series of shell-crosslinked nanoparticles (SCKs) have been constructed by grafting a copper chelating agent (DOTAlysine) onto amphiphilic block copolymers PAA-*b*-PS, self assembling the functionalized block copolymer precursors into micelles, and crosslinking the micellar corona to afford the expected nanoobjects. These pre-DOTAlysine-SCKs showed impressive results on ^{64}Cu radiolabeling (~ 400 copper atoms per spherical nanoparticle).

Among the molecular imaging modalities, PET is widely used as a powerful diagnostic tool by clinicians and scientists.[1] Compared with other imaging methods, it bears the advantages of high sensitivity (the level of detection approaches 10^{-11} M of tracer) and isotropism (*i.e.*, ability to detect expression accurately, regardless of tissue depth), which provide reliability for quantitative imaging analyses of *in vivo* abnormalities. As the pharmaceutical industry began applying PET imaging for assisting drug discovery,[2] small animal PET scanners with spatial resolution up to 1 mm were developed and have been considered to be one of the major achievements for PET technology during the past two decades.[3] ^{64}Cu is an attractive radionuclide for PET imaging because of its suitable half-life ($t_{1/2}$ = 12.7 h) and positron emission energy (0.65 MeV), as well as the relatively convenient radiolabeling *via* coordination with specially designed ligands (chelators).[4] The formation of thermodynamically-stable metal complexes reduces the copper binding with plasma proteins which minimizes its non-specific background activity and its accumulation and resultant toxicity in the liver and kidney.[5] Under the present instrumental conditions, optimizations and improvements of the specific activity of radiopharmaceuticals are of special interest to ^{64}Cu-based PET systems for achieving high quality images even at low doses, especially when the targets can be readily saturated *in vivo*.[3e] One practical resolution is to encapsulate or conjugate the chelating agents with nanocarriers, which have already been utilized by many research groups[6] including ourselves[7, 8] and have been found to exhibit exciting potential in both high loading capacities and redirection of the bio-distributions of small molecule ligands (*e.g.* for tissue targeting) or guests (*e.g.* for pharmaceutical effect).[9]

Our research has focused upon SCKs[10] as the nanoscale framework for the attachment of macrocyclic chelators and labeling by ^{64}Cu radionuclides. SCKs have been established from the self-assembly of amphiphilic block copolymers to afford micelles with core-shell morphology that are then covalently crosslinked throughout the shell domain. Recently, it was confirmed that by tuning the nanoparticle properties, especially the size and rigidity, increased *in vivo* circulation times and improved bio-distributions could be reached for ^{64}Cu-TETA SCK conjugates.[8] Although these preliminary results are promising, several challenges require further investigations. Among them, efficient radiolabeling takes the highest priority. Previously, the direct conjugation of macrocyclic chelators onto pre-established SCKs afforded limited coupling and radiolabeling yields, due to steric and electrostatic factors.[8, 11] As part of our ongoing efforts, we now report an alternative strategy to construct chelator-SCK conjugates with high radiolabeling efficiencies, which is expected to lead to nanoscale objects that can be administered in small quantities for ultra-sensitive PET imaging.

[*] Prof. M. J. Welch, Prof. K. L. Wooley, Dr. A. Hagooly, Dr. R. Rossin
Mallinckrodt Institute of Radiology
Washington University School of Medicine
Saint Louis, MO 63110 (USA)
E-mail: welchm@mir.wustl.edu; klwooley@wustl.edu
Prof. K. L. Wooley, G. Sun, Dr. J. Xu, Z. Li
Center for Materials Innovation and Department of Chemistry
Washington University in Saint Louis
Saint Louis, MO 63130 (USA)
Dr. D. A. Moore
Mallinckrodt Inc.
Saint Louis, MO 63134 (USA)
Prof. C. J. Hawker
Materials Research Laboratory
University of California at Santa Barbara
Santa Barbara, CA 93106 (USA)

[**] G.S., J.X., and A.H. contributed equally. This material is based upon work supported by the National Heart Lung and Blood Institute of the National Institutes of Health as a Program of Excellence in Nanotechnology (HL080729). The production of ^{64}Cu is supported by the National Cancer Institute (CA86307). The authors thank Ms. N. Kohrt and Prof. S. Sakiyama-Elbert for their assistance with DLS measurements, and Mr. M. G. Veith for TEM imaging.

ADVANCED MATERIALS

SCKs used in this study were comprised of polystyrene (PS) and poly(acrylic acid) (PAA), a particle composition previously demonstrated to have long blood circulation times[8] and characteristic low cytotoxicity and low immunogenicity when crosslinked with 2,2′-(ethylenedioxy)-bis(ethylamine).[12] The particle sizes were controlled by the relative balance of hydrophobic PS block length *vs.* the hydrophilic PAA segment.[13] The amphiphilic block copolymer precursors (PAA-*b*-PS) were acquired *via* sequential living radical polymerization of *tert*-butyl acrylate and styrene, followed by acidolysis of the *tert*-butyl ester protecting groups. In all cases, the block copolymers had well-defined structures and narrow polydispersities (PDI < 1.20).

As shown in Scheme 1, a lysine derivative of 1,4,7,10-tetraazocyclododecane-*N,N′,N″,N‴*-tetraacetic acid (DOTA), DOTAlysine, was grafted onto the amphiphilic PAA-*b*-PS block polymer precursors, with a fixed hydrophilic PAA segment length (DP_n = 60) and varied hydrophobic PS segment lengths (DP_n = 30, 60, 140). Conventional amidation chemistry was employed in organic solvent to afford *ca.* 65 to 75% isolated yield, for which the coupling yields were > 85%. After purification by dialysis against water and lyophilization, the numbers of DOTAlysines per polymer chain were determined by ^{1}H NMR spectroscopy analyses. For PAA_{60}-*b*-PS_{30} and PAA_{60}-*b*-PS_{60} block copolymers, the grafting numbers were 2, 4, and 7, for three different samples. Grafting more DOTAlysines (> 10 DOTAlysines/chain) was also attempted, but the resulting DOTAlysine-*g*-copolymers suffered from poor solubility in organic solvents and generated nanoparticles with broad size distributions. The same problem was encountered for the PAA_{60}-*b*-PS_{140} after coupling 7 DOTAlysines, so only 2 and 4 DOTAlysines/chain were studied.

Each amphiphilic block copolymer was assembled into micelles in aqueous solution by a standard micellization pro-

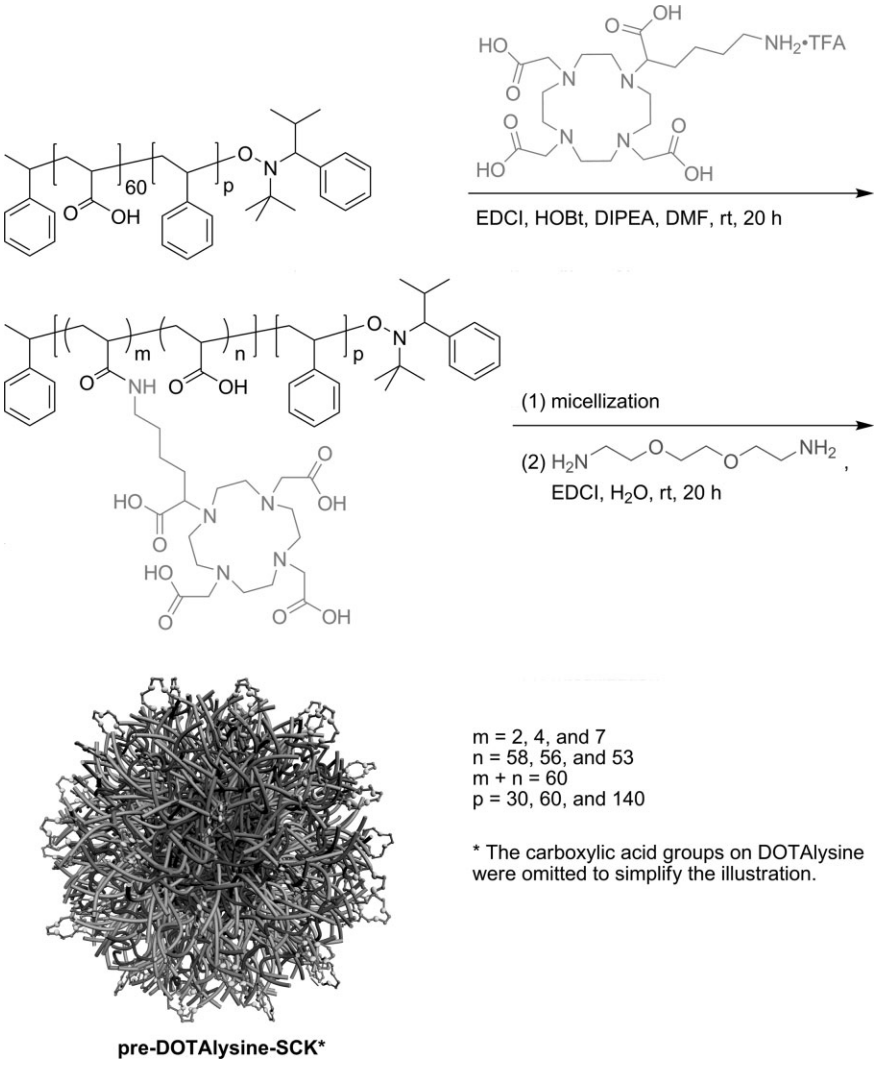

Scheme 1. A two-step synthetic route was developed for the preparation of pre-DOTAlysine-SCKs: (1) labelling of three different amphiphilic block copolymers, PAA_{60}-*b*-PS_p, with three different levels of DOTAlysine; (2) their self-assembly into micelles in water and shell crosslinking to two different extents. Overall, 8 micelles and 16 SCKs resulted from this scheme (see also Table 1).

tocol[14] and crosslinked throughout the shell layer to differing degrees (20% and 50%, according to the chemical stoichiometry). A series of micelles and SCKs having different dimensions and shell properties (electrostatic character, permeability, and residual carboxylic acid concentrations) was obtained and characterized by dynamic light scattering (DLS) and transmission electron microscopy (TEM; Table 1 and Figure 1).

Based upon the TEM image analysis, the number of grafting DOTAlysines greatly influenced the morphologies of the nanoparticles. All pre-DOTAlysine-SCKs constructed from the three different amphiphilic block copolymers, each having 2 DOTAlysines/polymer chain (**SCK1**-**3** having undergone 20% crosslinking, and **SCK9**-**11**, with 50% crosslinking) exhibited spherical morphologies with relatively narrow particle size distributions. This similarity could be attributed to the fact that the small percentage of modification (< 4%) across the PAA backbone did not generate significant variation over the entire block copolymer properties, *i.e.* the balance between the hydrophilic and hydrophobic blocks remained little affected. When p = 30 or 60, the pre-DOTAlysine$_2$-*g*-PAA$_{58}$-*b*-PS$_p$ polymers gave uniform assembly (**SCK1**, **SCK2**, **SCK9**, and **SCK10**) to afford SCK dimensions that were in agreement with control SCKs (Figure 1i and 1j), prepared from PAA$_{60}$-*b*-PS$_{30}$ and PAA$_{60}$-*b*-PS$_{60}$, respectively. In these cases, the loss of hydrophilicity (*i.e.*, transformation of carboxylic acid to amide linkage) and the increased steric repulsion caused by the rigid macrocyclic moiety of DOTAlysine could be partially compensated by the *ca.* 10% increase of carboxylic acid residues (from DOTAlysine) over the length of the PAA$_{60}$ segments. In contrast, the DOTAlysine-functionalized amphiphilic block copolymers with the longest PS chain segment, DOTAlysine$_2$-*g*-PAA$_{58}$-*b*-PS$_{140}$ underwent assembly into unusually small micelles to afford **SCK3** and **SCK11** that were significantly smaller in size and aggregation number than was the control assembly from PAA$_{60}$-*b*-PS$_{140}$ (Figure 1k). We are still investigating the reasons for the atypical assembly for these block copolymers.

Table 1. Characterization data for pre-DOTAlysine-SCKs and control SCK samples (lacking DOTA functionalities).

Sample [a] (Extents of Crosslinking)	$(D_h)_n$ [b] [nm]	D_{av} [c] [nm]	(DOTAlysine$_m$-*g*-PAA$_n$)-*b*-PS$_p$			N_{agg} [e]
			m	n	p	
SCK1 (20%)	21 ± 3	11 ± 1	2	58	30	125
SCK2 (20%)	21 ± 3	16 ± 2	2	58	60	240
SCK3 (20%)	21 ± 6	11 ± 2	2	58	140	40
SCK4 (20%)	21 ± 3	12 ± 2 [d]	4	56	30	160 [d]
SCK5 (20%)	47 ± 7	19 ± 2 [d]	4	56	60	340 [d]
SCK6 (20%)	17 ± 2	11 ± 2	4	56	140	40
SCK7 (20%)	26 ± 6	11 ± 2	7	53	30	125
SCK8 (20%)	25 ± 6	19 ± 2	7	53	60	400
SCK9 (50%)	21 ± 3	11 ± 1	2	58	30	125
SCK10 (50%)	24 ± 3	16 ± 2	2	58	60	240
SCK11 (50%)	13 ± 4	12 ± 2	2	58	140	40
SCK12 (50%)	22 ± 4	15 ± 2 [d]	4	56	30	160 [d]
SCK13 (50%)	43 ± 5	18 ± 3 [d]	4	56	60	340 [d]
SCK14 (50%)	17 ± 4	13 ± 2	4	56	140	40
SCK15 (50%)	24 ± 5	11 ± 2	7	53	30	125
SCK16 (50%)	28 ± 4	19 ± 2	7	53	60	400
Control1 (50%)	18 ± 2	11 ± 1	0	60	30	125
Control2 (50%)	22 ± 1	17 ± 1	0	60	60	240
Control3 (50%)	34 ± 4	25 ± 1	0	60	140	330

[a] All samples were dispersed in 5.0 mM pH 7.3 PBS (with 5.0 mM NaCl) buffer solutions. [b] The number-averaged hydrodynamic diameters ($(D_h)_n$) were determined by DLS. Samples were passed through PVDF filters with 220 nm average pore size before conducting DLS measurements. [c] The TEM average diameter (D_{av}) values were measured for the nanoparticle cores. [d] Only spherical nanoparticles were counted. [e] The aggregation numbers (N_{agg}) were calculated based upon TEM micrographs.

For pre-DOTAlysine-SCKs with *ca.* 4 DOTAlysines/chain (20% crosslinking for **SCK4**-**6** and 50% crosslinking for **SCK12**-**14**), their morphologies became much more complex. As the DOTAlysine$_4$-*g*-PAA$_{56}$-*b*-PS$_{30}$ was assembled, in addition to the major spherical morphology (> 80%), small rod-like structures appeared with *ca.* 60 nm length (Figure 1b). Such unusual observation became extreme for SCKs prepared from DOTAlysine$_4$-*g*-PAA$_{56}$-*b*-PS$_{60}$, in which half of the nanoobjects were rods with average lengths of *ca.* 100 nm (Figure 1e). It is unclear whether the sphere-to-rod morphological transition results from interruptions on the local Coulomb interactions within the nanostructures, a hydrophilicity change in the shell domain, or a combination of these factors. Detailed studies to better understand the "driving force" of this uncommon morphological transition are currently underway. In the case of SCKs from DOTAlysine$_4$-*g*-PAA$_{56}$-*b*-PS$_{140}$ (**SCK6** and **SCK14**), spheres still remained dominant, but their particle size distributions were broad (Figure 1h).

Interestingly, as the grafting DOTAlysine number continued to increase, the four SCKs (**SCK7**, **SCK8**, **SCK16**, and **SCK17**) from DOTAlysine$_7$-*g*-PAA$_{53}$-*b*-PS$_{30(60)}$ returned to the more thermodynamically favorable spherical morphology. It is surprising that, even at this high proportion of modification (*i.e.*, the introduction of *ca.* 21 additional carboxylic acid groups per hydrophilic chain segment and the concomitant increased hydrophilic ratio and increased steric effects) along the polymer backbones, their assembly sizes and shapes remained similar to the control SCKs. Again, the block copolymer having the longest PS block length and coupling of *ca.* 7 DOTAlysines per polymer was unusual, in that it experienced poor solubility and could not be assembled into uniform micelles.

Radiolabeling of these micelles and their corresponding SCKs with ^{64}Cu were investigated thoroughly. To simplify the influence of functional group transformation along the DOTAlysine grafts (carboxylic acids to amides) during the crosslinking process, which might affect their efficient chelation with ^{64}Cu, no greater than 10 mol% ^{64}Cu (relative to the DOTAlysine grafts) were used to ensure full complexation of the copper cations. All the pre-DOTAlysine-SCKs/micelles exhibited high specific activity (Figure 2) compared with the SCKs prepared by coupling the DOTA onto pre-established nanoparticles (post-DOTA-SCKs, Control4 in

ADVANCED MATERIALS

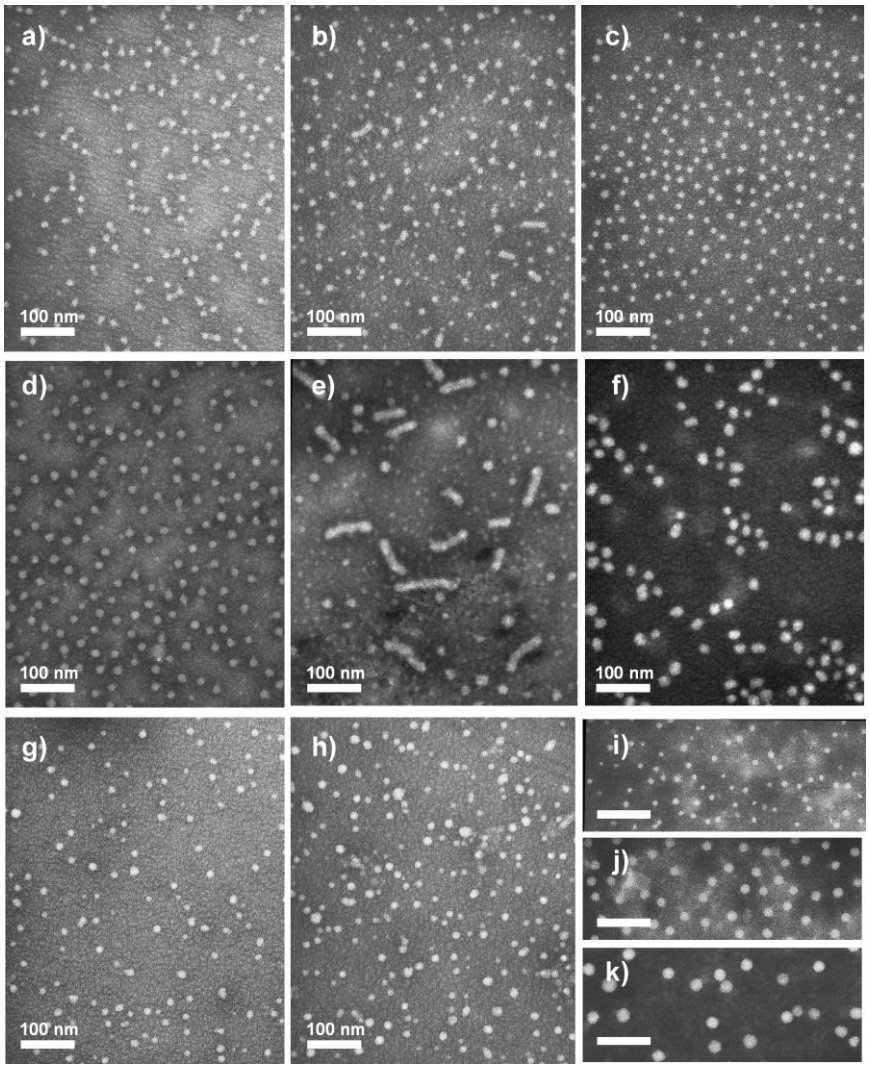

Figure 1. TEM micrographs of 50% crosslinked SCKs prepared from DOTAlysine$_m$-*g*-PAA$_n$-*b*-PS$_p$ block copolymer precursors: (a), (b), (c), and (i) are images of **SCK9**, **SCK12**, **SCK15**, and **Control1**, prepared from PAA$_{60}$-*b*-PS$_{30}$ with 2, 4, 7, and 0 DOTAlysine grafts, respectively; (d), (e), (f), and (j) are images of **SCK10**, **SCK13**, **SCK16**, and **Control2**, prepared from PAA$_{60}$-*b*-PA$_{60}$ with 2, 4, 7, and 0 DOTAlysine grafts, respectively; (g), (h), and (k) are images of **SCK11**, **SCK14**, and **Control3**, prepared from PAA$_{60}$-*b*-PA$_{140}$ with 2, 4, and 0 DOTAlysine grafts, respectively. Scale bars in (i), (j), and (k): 100 nm.

Figure 2).[11] The specific activities of the pre-DOTAlysine-SCKs increased by 10 to 40 fold. This high radiolabeling on a per particle basis creates an opportunity for reliable use with administration of a minimum amount of polymeric nanoparticles for *in vivo* PET imaging.

The specific activity and the number of effective DOTAlysines per SCK did not follow the expected tendency, which would be an increase in labeling with an increase in DOTAlysine grafting density. Rather, it appeared that the proportion of DOTAs available for ^{64}Cu chelation reached a "saturation point" after 4 DOTAlysine grafts per polymer chain. Since not all grafting DOTAlysines were located on the particle surface, the membrane-like structures within the shell regions of SCKs[15] might hinder the formation of ^{64}Cu-DOTAlysine complexes due to steric crowding and prevention of the DOTAlysine macrocyclic from assuming a configuration amenable to stable ^{64}Cu coordination.[16] It is uncertain whether morphological differences (sphere *vs.* rod) also play a role.

Moreover, for SCKs prepared from a fixed DOTAlysine graft number per polymer chain (Figure 2), it was found that: (i) as the extents of crosslinking increased (from 0% to 50%), less DOTAlysines were available for coordinating with copper; (ii) as the proportion of the hydrophilic PAA comprising the entire nanostructure decreased, so did the number of effective DOTAlysines and the overall specific activity. The lower permeability within the shell domains of the SCKs having higher extents of crosslinking[15] could hinder the diffusion of ^{64}Cu to approach the DOTAlysine chelators located throughout the sub-surface and deep-shell areas. For instance, the number of effective DOTAlysines per DOTAlysine$_7$-*g*-PAA$_{53}$-*b*-PS$_{30}$ chain determined by isotopic dilution experiments (see Experimental) was ca. 2.8, much lower than 7.0, which was determined by ^{1}H NMR analysis. An additional explanation might be that higher degrees of crosslinking could reduce the number of intact DOTA units, through consumption of their carboxylic acids. The amidation chemistry during crosslinking may consume carboxylic acid residues without selectivity between the PAA polymer backbone and the DOTAlysine moieties. The resulting local environmental interruption around DOTA moieties could negatively affect complex formation. The second trend observed further suggests the complexities on the self-assembly behavior of DOTAlysine-*g*-PAA-*b*-PS block copolymers. The lower radiolabeling efficiency on micelles and SCKs established from the longer hydrophobic PS block (while the DOTAlysine-*g*-PAA segment was invariable) could be related with their atypical morphological characteristics (vide supra). Nevertheless, all micelles and SCKs prepared from DOTAlysine-*g*-PAA-*b*-PS exhibited high radiolabeling results, providing a library of nanoparticles with varying characteristic parameters to be employed for PET imaging when a minimum amount of imaging agent is needed.

It is noteworthy that this grafting strategy affords nanoobjects with remarkably improved radiolabeling efficiencies, relative to the post-functionalization of pre-established

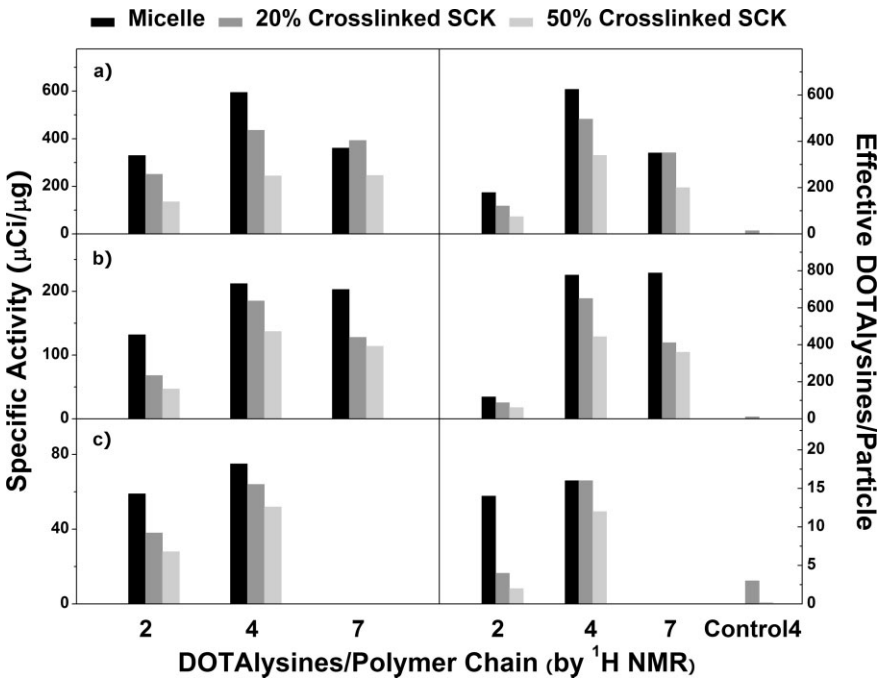

Figure 2. Radiolabelling results for pre-DOTAlysine-SCKs: (a) SCKs from functionalized PAA_{60}-*b*-PS_{30}; (b) SCKs from functionalized PAA_{60}-*b*-PS_{60}; (c) SCKs from functionalized PAA_{60}-*b*-PS_{140}. The numbers of effective DOTAlysines/particle (with ± 5% standard deviation) were obtained from the numbers of effective DOTAlysines/polymer chain (determined from isotopic dilution experiments, see Experimental) and the calculated particle aggregation number (Table 1). **Control4** were post-DOTA-SCKs [11].

SCKs,[11] but also introduces complications with the assembling process, presenting unusual morphologies in some cases. More efforts are being devoted to investigate these morphological variations. Although micelles give the highest radiolabeling, their stability concerns, i.e., stable architectures exist only above their critical micelle concentrations, remain challenging for *in vivo* applications.[17] Considering both the radiolabeling results and the SCK morphological properties, we conclude, tentatively, that the current optimum sample for in vivo PET imaging are SCKs having 20% shell crosslinking and prepared from PAAn-*b*-PSp containing ca. 2 DOTAlysine per polymer chain.

In summary, we have developed a new strategy to construct shell crosslinked nanoparticles, containing large numbers of DOTAlysines per particle (> 400) that were accessible for ^{64}Cu radiolabeling. These nanoparticles originated from conveniently prepared DOTAlysine-*g*-PAA-*b*-PS block copolymer precursors. The morphology of these pre-DOTAlysine-SCKs was, however, complicated by the number of DOTAlysine grafts per polymer chain. Nonetheless, the ^{64}Cu–complexed pre-DOTAlysine-SCK nanoparticles showed impressive specific activities (ca. 400 μCi μg^{-1}), which suggest that these nanoparticles might be used to develop highly sensitive in vivo PET tracers at low administering doses. This "pre-grafting" strategy may also be employed to couple other molecules for targeting interested epitopes and/or for improving the in vivo bio-distribution of nanoobjects.

Experimental

PAA-b-PS Block Copolymer Synthesis: All block copolymers were synthesized by acidolysis of P*t*BA-*b*-PS precursors, which were prepared by sequential polymerization of *tert*-butyl acrylate and styrene *via* nitroxide mediated radical polymerization (NMP), with trifluoroacetic acid (TFA) as reported in the literature [18].

General Procedure for DOTAlysine-g-PAA-b-PS Synthesis: Grafting DOTAlysines onto PAA-*b*-PS by amidation involved the following: To a round-bottom flask equipped with a magnetic stir bar, was added a sample of PAA-*b*-PS block copolymer and anhydrous *N*,*N*-dimethylformamide (DMF). The mixture was stirred for 1 h at room temperature to ensure that a clear and homogeneous solution was obtained. To this solution, was added 1-[3′-(dimethylamino)propyl]-3-ethylcarbodiimide methiodide (EDCI) and 1-hydroxybenzotriazole (HOBt) and the reaction mixture was stirred for 1 h at room temperature. Finally, a pre-mixed solution of DOTAlysine·TFA and *N*,*N*-diisopropylethylamine (DIPEA) in anhydrous DMF was added and the reaction mixture was further stirred for 20 h at room temperature. The reaction mixture was then transferred to pre-soaked dialysis tubing (MWCO *ca.* 6000 to 8000 Da) and dialyzed against nano-pure H_2O (18.0 MΩ cm, pre-treated with Chelex100) for 4 d to remove the organic solvent and small molecule by-products. The aqueous solution was then lyophilized to afford the product as white solid.

General Procedure for the Micellization of DOTAlysine-g-PAA-b-PS: To a round-bottom flask equipped with a magnetic stir bar, was added DOTAlysine-*g*-PAA-*b*-PS, followed by anhydrous DMF. The mixture was sonicated for 10 min and stirred for 2 h at room temperature to ensure that a clear and homogeneous solution (final conc., *ca.* 1.0 mg mL^{-1}) had formed. To this solution, was added dropwise *via* a syringe pump at a rate of 15.0 mL h^{-1}, an equal volume of nano-pure H_2O (18.0 MΩ cm) and the mixture was further stirred for 16 h at room temperature. Finally, the solution was transferred to pre-soaked dialysis tubing (MWCO *ca.* 6000 to 8000 Da) and dialyzed against nano-pure H_2O (18.0 MΩ cm, pre-treated with Chelex100) for 4 d to afford a clear solution of micelles.

General Procedure for the Preparation of Pre-DOTAlysine-SCKs: To a 250 mL round-bottom flask equipped with a magnetic stir bar, was added a solution of DOTAlysine-*g*-PAA-*b*-PS micelles in nano-pure H_2O (18.0 MΩ cm) (50.0 mL, 0.054 mmol of carboxylic acid residues). To this solution was added dropwise over 10 min, a solution of 2,2′-(ethylenedioxy)-bis(ethylamine) (0.9 mg, 0.006 mmol for 20% crosslinking extent; or 2.2 mg, 0.015 mmol for 50% crosslinking extent) in nano-pure H_2O (18.0 MΩ cm) (2.0 mL). The reaction mixture was allowed to stir for 2 h at room temperature. To this solution was added, dropwise *via* a syringe pump over 1 h, a solution of EDCI (4.0 mg, 0.014 mmol for 20% crosslinking extent; or 10.0 mg, 0.034 mmol for 50% crosslinking extent) in nano-pure H_2O (18.0 MΩ cm) (2.0 mL) and the reaction mixture was further stirred for 16 h at room temperature. Finally, the reaction mixture was transferred to pre-soaked dialysis tubing (MWCO *ca.* 6000 to 8000 Da) and dialyzed against 5.0 mM PBS (pH 7.3, with 5.0 mM NaCl, pre-treated with Chelex100) for 5 d to remove the small molecule by-products and afford aqueous solutions of pre-DOTAlysine-SCKs.

^{64}Cu labeling and isotopic dilution experiments of the pre-DOTAlysine-SCKs: A 100 μL pre-DOTAlysine-SCK solution in 5.0 mM PBS

ADVANCED MATERIALS

(pH 7.3, with 5.0 mM NaCl, 0.2–0.3 mg mL^{-1}) was diluted with 100 μL of 0.1 M ammonium acetate buffer (pH 5.5) and to this solution, $^{64}Cu(OAc)_2$ was added (*ca.* 1.0 mCi). The resulting solution was incubated at 43 °C for 2 h, and then subjected to DTPA challenge. The labeling yield was determined by radio-TLC on ITLC-SG plates using methanol/$CH_3CO_2NH_4$ (aq) as eluent. The number of effective DOTAlysines/polymer chain was determined by isotopic dilution experiments. A series of known amounts of "hot plus cold" copper (Cu^{2+} solution spiked with ^{64}Cu) were added to several 100 μL SCK solutions respectively. After a 2 h incubation at 43 °C and DTPA challenge, each solution aliquot was analyzed by radio-ITLC to determine the number of effective DOTAlysine per polymer chain, as previously reported [8,19].

Received: August 8, 2007

[1] a) M. E. Phelps, *Proc. Natl. Acad. Sci. USA.* **2000**, *97*, 9226. b) R. Weissleder, U. Mahmood, *Radiology* **2001**, *219*, 316. c) S. S. Gambhir, *Nat. Rev. Cancer* **2002**, *2*, 683.

[2] a) G. Lappin, R. C. Garner, *Nat. Rev. Drug Discov.* **2003**, *2*, 233. b) C. M. L. West, T. Jones, P. Price, *Nat. Rev. Cancer* **2004**, *4*, 457. c) J. Wang, L. Maurer, *Curr. Top. Med. Chem.* **2005**, *5*, 1053. d) W. A. Weber, *J. Nucl. Med.* **2006**, *47*, 735.

[3] a) H. I. Kornblum, S. R. Cherry, *J. Clin. Pharmacol.* **2001**, *41*, 55S. b) F. C. Arion, *Eur. J. Nucl. Med. Mol. Imaging* **2002**, *29*, 98. c) D. J. Rowland, J. S. Lewis, M. J. Welch, *J. Cell. Biochem.* **2002**, *87*, 110. d) S. Weber, A. Bauer, *Eur. J. Nucl. Med. Mol. Imaging* **2004**, *31*, 1545. e) B. Van Den Bossche, C. Van De Wiele, *J. Clin. Oncol.* **2004**, *22*, 3593. f) V. Sossi, T. J. Ruth, *J. Neural Transm.* **2005**, *112*, 319. g) G. C. Li, F. He, C. C. Ling, *Int. J. Hyperthermia* **2006**, *22*, 215. h) S. R. Cherry, *J. Nucl. Med.* **2006**, *47*, 1735.

[4] a) C. J. Anderson, M. J. Welch, *Chem. Rev.* **1999**, *99*, 2219. b) R. Laforest, D. J. Rowland, M. J. Welch, *IEEE Trans. Nucl. Sci.* **2002**, *49*, 2119. c) S. V. Smith, *J. Inorg. Biochem.* **2004**, *98*, 1874. d) T. J. Wadas, E. H. Wong, G. R. Weisman, C. J. Anderson, *Curr. Pharm. Des.* **2007**, *13*, 3.

[5] C. A. Boswell, X. Sun, W. Niu, G. R. Weisman, E. H. Wong, A. L. Rheingold, C. J. Anderson, *J. Med. Chem.* **2004**, *47*, 1465.

[6] a) V. S. Trubetskoy, *Adv. Drug Deliv. Rev.* **1999**, *37*, 81. b) V. P. Torchilin, *Adv. Drug Deliv. Rev.* **2002**, *54*, 235. c) I. Brigger, C. Dubernet, P. Couvreur, *Adv. Drug Deliv. Rev.* **2002**, *54*, 631. d) A. N. Lukyanov, V. P. Torchilin, *Adv. Drug Deliv. Rev.* **2004**, *56*, 1273. e) L. Brannon-Peppas, J. O. Blanchette, *Adv. Drug Deliv. Rev.* **2004**, *56*, 1649.

[7] R. Rossin, D. Pan, J. L. Turner, X. Sun, K. L. Wooley, M. J. Welch, *J. Nucl. Med.* **2005**, *46*, 1210.

[8] X. Sun, R. Rossin, J. L. Turner, M. L. Becker, M. J. Joralemon, M. J. Welch, K. L. Wooley, *Biomacromolecules* **2005**, *6*, 2541.

[9] a) G. M. L. Samuel, A. Wickline, *J. Cell. Biochem.* **2002**, *87*, 90. b) A. Mitra, A. Nan, B. R. Line, H. Ghandehari, *Curr. Pharm. Des.* **2006**, *12*, 4729.

[10] a) K. L. Wooley, *J. Polym. Sci. A: Polym. Chem.* **2000**, *38*, 1397. b) Y. Li, G. Sun, J. Xu, K. L. Wooley, in *Nanotechnology in Therapeutics: Current Technology and Applications*, (Eds: N. A. Peppas, J. Z. Hilt, J. B. Thomas), Horizon Bioscience, Norfolk, U. K. **2007**, Ch. 16.

[11] J. Xu, G. Sun, R. Rossin, A. Hagooly, Z. Li, K. Fukukawa, B. M. Messmore, D. A. Moore, M. J. Welch, C. J. Hawker, K. L. Wooley, *Macromolecules* **2007**, *40*, 2971.

[12] M. L. Becker, J. Liu, K. L. Wooley, *Biomacromolecules* **2005**, *6*, 220.

[13] a) K. B. Thurmond, T. Kowalewski, K. L. Wooley, *J. Am. Chem. Soc.* **1997**, *119*, 6656. b) H. Huang, T. Kowalewski, E. E. Remsen, R. Gertzmann, K. L. Wooley, *J. Am. Chem. Soc.* **1997**, *119*, 11653.

[14] a) L. Zhang, A. Eisenberg, *Science* **1995**, *268*, 1728. b) L. Zhang, A. Eisenberg, *J. Am. Chem. Soc.* **1996**, *118*, 3168.

[15] K. S. Murthy, Q. Ma, C. G. Clark, Jr., E. E. Remsen, K. L. Wooley, *Chem. Commun.* **2001**, 773.

[16] A. Riesen, M. Zehnder, T. A. Kaden, *Helv. Chim. Acta* **1986**, *69*, 2067.

[17] R. Savic, T. Azzam, A. Eisenberg, D. Maysinger, *Langmuir* **2006**, *22*, 3570.

[18] R. K. O'Reilly, M. J. Joralemon, K. L. Wooley, C. J. Hawker, *Chem. Mater.* **2005**, *17*, 5976.

[19] D. W. McCarthy, R. E. Shefer, R. E. Klinkowstein, L. A. Bass, W. H. Margeneau, C. S. Cutler, C. J. Anderson, M. J. Welch, *Nucl. Med. Biol.* **1997**, *24*, 35.